ADVANCES IN ATMOSPHERIC SCIENCES, VOL. 35, NOVEMBER 2018, 1347–1361

• **Original Paper** •

Modulation of the Intensity of Nascent Tibetan Plateau Vortices by Atmospheric Quasi-Biweekly Oscillation

Lun LI*[1], Renhe ZHANG[2,3], Min WEN[1], and Jianping DUAN[4]

[1]*State Key Laboratory of Severe Weather, Chinese Academy of Meteorological Sciences, Beijing* 100081*, China*
[2]*Institute of Atmospheric Sciences, Fudan University, Shanghai* 200433*, China*
[3]*Chinese Academy Science Center for Excellence in Tibetan Plateau Earth Sciences, Beijing* 100101*, China*
[4]*Institute of Atmospheric Physics, Chinese Academy Science, Beijing* 100029*, China*

(Received 10 March 2018; revised 28 May 2018; accepted 30 May 2018)

ABSTRACT

The modulation of the intensity of nascent Tibetan Plateau vortices (ITPV) by atmospheric quasi-biweekly oscillation (QBWO) is investigated based on final operational global analysis data from the National Centers for Environmental Prediction. The spatial and temporal distributions of the ITPV show distinct features of 10–20-day QBWO. The average ITPV is much higher in the positive phases than in the negative phases, and the number of strong TPVs is much larger in the former, with a peak that appears in phase 3. In addition, the maximum centers of the ITPV stretch eastward in the positive phases, indicating periodic variations in the locations where strong TPVs are generated. The large-scale circulations and related thermodynamic fields are discussed to investigate the mechanism by which the 10–20-day QBWO modulates the ITPV. The atmospheric circulations and heating fields of the 10–20-day QBWO have a major impact on the ITPV. In the positive QBWO phases, the anomalous convergence at 500 hPa and divergence at 200 hPa are conducive to ascending motion. In addition, the convergence centers of the water vapor and the atmospheric unstable stratification are found in the positive QBWO phases and move eastward. Correspondingly, condensational latent heat is released and shifts eastward with the heating centers located at 400 hPa, which favors a higher ITPV by depressing the isobaric surface at 500 hPa. All of the dynamic and thermodynamic conditions in the positive QBWO phases are conducive to the generation of stronger TPVs and their eastward expansion.

Key words: quasi-biweekly oscillation, Tibetan Plateau vortex, modulation

Citation: Li, L., R. H. Zhang, M. Wen, and J. P. Duan, 2018: Modulation of the intensity of nascent Tibetan Plateau vortices by atmospheric quasi-biweekly oscillation. *Adv. Atmos. Sci.*, **35**(11),1347–1361, https://doi.org/10.1007/s00376-018-8057-y.

1. Introduction

Tibetan Plateau vortices (TPVs) are important rain producers originating over the Tibetan Plateau and are defined at 500 hPa (Ye and Gao, 1979). TPVs always form over the central-western Tibetan Plateau from June to August, and the number of newly formed TPVs peaks in June. They are mesoscale systems with typical horizontal and vertical scales of 400–800 km and 2–3 km, respectively (Ye and Gao, 1979; Lhasa Group for Tibetan Plateau Meteorology Research, 1981; Luo, 2012; Luo et al., 1994). Although many TPVs dissipate over the Tibetan Plateau, some can move eastward off the plateau under certain conditions (Wang et al., 2009). Those TPVs that move off the plateau are closely related to the genesis of southwest vortices in southwestern China (Li et al., 2017), and lots of heavy rainfall and disastrous weather events to the east of the Tibetan Plateau are triggered by such TPVs (Ye and Gao, 1979; Qiao and Zhang, 1994; Li, 2002).

The formation stages of TPVs are the focus of the present work. Features of the large-scale circulations and the related thermodynamic factors have been revealed in previous studies. A cyclonic wind shear at 500 hPa, and the ascending motion related to the convergence at 500 hPa and divergence at 200 hPa, are conducive to the occurrence of TPVs (Li et al., 2011, 2014a). Water vapor over the Arabian Sea and western India leads to favorable conditions for the generation of TPVs (Yu and He, 2001). In addition, some TPVs are triggered by shear lines (Tu and He, 2010). The role of thermodynamic fields in the initial processes of the TPVs has been investigated. The condensational latent heat is considered to be the most influential factor in some studies (Dell'Osso and Chen, 1986; Wang, 1987; Li et al., 2011, 2014b; Zheng et al., 2013); while in other studies, the effect of surface sensible heat is highlighted (Lhasa Group for Tibetan Plateau Meteorology Research, 1981; Shen et al., 1986; Luo et al., 1991; Li, 2002), and the dynamic effect is thought to be less important

* Corresponding author: Lun LI
Email: lilun@cma.gov.cn

(Luo and Yang, 1992; Chen et al., 1996).

Atmospheric intraseasonal oscillation (ISO) plays an important role in medium- and long-term weather forecasts and, accordingly, the influence of ISO on TPVs has been explored in some studies. Previous studies have revealed that ISO significantly modulates the activities of TPVs, as follows. The positive phases of the 10–20-day ISO over the eastern Tibetan Plateau supply favorable conditions for the eastward movement of TPVs (Li et al., 2018a). In addition, the generation of TPVs has obvious active and suppressed periods, exhibiting a close relationship with ISO (Zhang et al., 2014; Li et al., 2018b). Sun and Chen (1994) suggested that the generation centers of TPVs are in accordance with the active centers of the 30–50-day ISO over the Tibetan Plateau. Thus, previous studies mainly concentrated on the modulation of the occurrence frequency of TPVs (Sun and Chen, 1994; Zhang et al., 2014; Li et al., 2018b) and the eastward movement of TPVs (Li et al., 2018a) by ISO, in which the main focus was on the temporal variation of TPVs, with the spatial distribution having not been investigated in any great depth. However, in general, few studies have investigated the influence of ISO on the activities of TPVs, and many aspects of this research field need to be explored. In the present work, similarly, the initial formation processes of TPVs are studied, but in the context of the intensity of nascent TPVs (ITPV) and over a longer period (2000–16). In addition, both the dynamic and thermodynamic features of ISO are considered, to reveal its effect on both the temporal and spatial distributions of the ITPV. Li et al. (2018b) showed that TPVs with different intensity respond differently to unfavorable background fields, and the survival probability of nascent TPVs is closely related to their intensity. Strong TPVs tolerate unfavorable backgrounds well, while weak ones are more sensitive and fragile, which to a large extent determines whether the newly formed TPV will survive or disappear. Therefore, the ITPV is an important subject worthy of research. The relationship between ISO and the spatial and temporal distributions of the ITPV, as well as the mechanism by which ISO modulates the ITPV, is analyzed in this study. The investigation of these issues benefits the prediction of the ITPV in different regions, and further provides information on the survival probability of nascent TPVs.

The data and methods are described in section 2. In section 3, the relationship between ISO and the ITPV is analyzed. Dynamic and thermodynamic processes are investigated in section 4, to reveal the underlying physical processes involved in the modulation of the ITPV by ISO. A discussion of the results and conclusions are given in section 5.

2. Data and methods

2.1. *Data and definition of TPVs*

Final operational global analysis (FNL) data, on a $1^\circ \times 1^\circ$ grid and at 6-h intervals during May–August in 2000–16, are used to determine the periodicity of 500-hPa vorticity over the Tibetan Plateau and investigate the temporal and spatial distributions of the ITPV, as well as the features of the large-scale circulations and heating fields. The data are provided by the Global Forecasting System of the National Centers for Environmental Prediction (NCEP), and can be downloaded at http://rda.ucar.edu/datasets/ds083.2. The intraseasonal signals are extracted by utilizing the Lanczos bandpass filter method (Duchon, 1979).

In the present study, based on the FNL gridded dataset, a cyclonic circulation in the 500-hPa wind fields over the Tibetan Plateau is selected as representative of a TPV. The occurrence frequency of TPVs derived from the FNL data according to this definition coincides well with that from observational data, based on the identification criteria created by the Lhasa Group for Tibetan Plateau Meteorology Research (1981) (Li et al., 2014a), implying good consistency between the two methods used to define TPVs and the reliability of the FNL data. The locations of TPVs emerging for the first time are marked as the generation locations of the nascent TPVs. The intensity of a TPV is calculated as the 500-hPa vorticity averaged over a $2^\circ \times 2^\circ$ region around its center (Li et al., 2018b).

2.2. *Water vapor flux*

The thermodynamic effect is closely related to the water vapor condition. Thus, the following equation from Rasmusson (1968) is used to calculate the vertically integrated water vapor flux ($\boldsymbol{A}$):

$$\boldsymbol{A} = \frac{1}{g}\int_{P_u}^{P_s} q\boldsymbol{V}\mathrm{d}p\,. \tag{1}$$

In Eq. (1), $\boldsymbol{V}$ denotes the horizontal wind vector, and q represents the specific humidity. P_s and P_u are the surface pressure and the pressure at the upper level, respectively. Here, $P_u = 100$ hPa.

2.3. *Atmospheric apparent heat source and apparent moisture sink*

The effect of diabatic heating on the ITPV is investigated by analyzing the features of the atmospheric apparent heat source (Q_1) and the apparent moisture sink (Q_2). The equations defining Q_1 and Q_2 (Yanai et al., 1973) are as follows:

$$Q_1 = c_p\left[\frac{\partial T}{\partial t} + \boldsymbol{V}\cdot\nabla T + \omega\left(\frac{P}{P_0}\right)^{\kappa}\frac{\partial\theta}{\partial p}\right]; \tag{2}$$

$$Q_2 = -L\left(\frac{\partial q}{\partial t} + \boldsymbol{V}\cdot\nabla q + \omega\frac{\partial q}{\partial p}\right). \tag{3}$$

Here, T is the temperature, and ω denote the vertical wind component in pressure coordinates, respectively. P_0 is the pressure of 1000 hPa. c_p represents the specific heat at constant pressure, and $\kappa \approx 0.286$. θ is the potential temperature. $L = 2.5\times10^6$ J kg^{-1}, denoting the latent heat of condensation, and q is the specific humidity.

3. Relationship between quasi-biweekly oscillation and the ITPV

The results in Fig. 1 enable us to investigate the periodicity of the atmosphere over the Tibetan Plateau. It shows that significant ISO is mainly concentrated within the period of 10–20 days. Therefore, the 10–20-day quasi-biweekly oscillation (QBWO) is statistically significant during May–August of 2000–16 over the Tibetan Plateau. A total of 72 life cycles of the standardized 10–20-day filtered 500-hPa vorticity averaged over the Tibetan Plateau, whose amplitudes are greater than 1.0, are selected. Subsequently, eight phases are defined according to Fig. 2, in which phases 2–4 are positive phases and 6–8 are negative phases.

The nascent TPVs are classified into four groups according to four ITPV levels. The numbers and ratios of TPVs in each level, and the average ITPV in each QBWO phase, are shown in Table 1. In each phase, the ratios of TPVs are calculated as the number of TPVs at each level divided by the total number of TPVs in this phase. According to Table 1, ITPV levels lower than 4×10^{-5} s^{-1}, between 4 and 6×10^{-5} s^{-1}, between 6 and 8×10^{-5} s^{-1}, and greater than 8×10^{-5} s^{-1} are named as Level 1, 2, 3, and 4, respectively. In general, the number of TPVs in Level 3 and 4 in the positive phases (154) is larger than that in the negative phases (72); this pattern is distinct from that in Level 1, in which the number of TPVs in the negative phases (89) is larger than that in the positive phases (71). In fact, the percentage of TPVs with intensity greater than 10×10^{-5} s^{-1} is the largest in phase 3 and smallest in phase 7, while TPVs with intensity less than 2×10^{-5} s^{-1} reaches a maximum in phase 7 and a minimum in phase 3 (not shown in the table). In addition, the average ITPV reaches a peak in phase 3, with a value of 6.2×10^{-5} s^{-1}, and a minimum in phase 7, with a value of 4.2×10^{-5} s^{-1}. The average ITPV in each positive phase is much greater than in the negative phase, implying that the conditions in the positive phases are more favorable for generating a higher intensity nascent TPV. Additionally, the percentage of strong TPVs is distinctly different across the eight phases, especially for phases 3 and 7. For TPVs occurring in phase 3, 56% are stronger than 6×10^{-5} s^{-1}, while the percentage is 25.6% in phase 7, indicating that the most favorable and unfavorable conditions for the generation of strong TPVs are in phase 3 and 7, respectively.

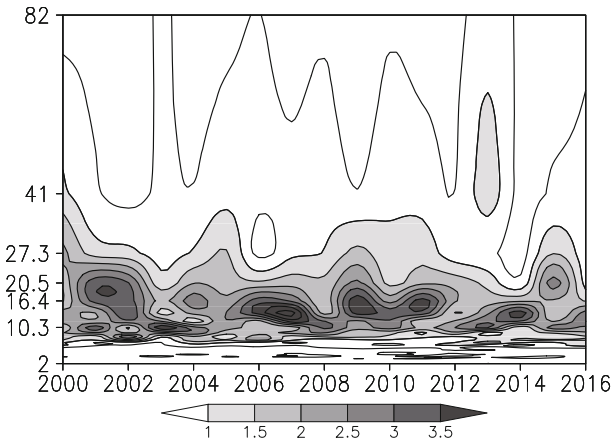

Fig. 1. Ratios of the power spectrum of 500-hPa vorticity averaged over the Tibetan Plateau (28°–37°N, 78°–103°E) and the red noise spectrum at the $\alpha = 0.05$ significance level. The interval of the contours is 0.5. Shading represents the periods passing the 95% confidence level.

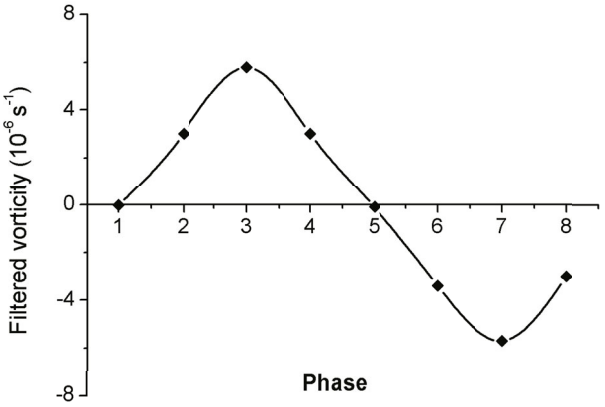

Fig. 2. Composites of 10–20-day filtered 500 hPa vorticity averaged over the Tibetan Plateau (28°–37°N, 78°–103°E) (unit: 10^{-6} s^{-1}). The *x*-axis indicates 8 QBWO phases.

To exhibit the spatial and temporal distributions of the ITPV, the locations of TPVs with different intensity occurring in the eight QBWO phases are exhibited in Fig. 3. In the positive phases, the maximum centers of the ITPV in each phase shift eastward from phases 1–4, with a peak appearing in phase 3 over the area (32°–36°N, 95°–100°E), indicating that both the temporal and spatial variations of the ITPV are closely related to the QBWO. In the negative phases, the loca-

Table 1. Numbers and ratios (in parentheses) of TPVs in four groups divided by the intensity of TPVs (i.e., the ITPV), and the average ITPV (bottom row; units: 10^{-5} s^{-1}) in each phase.

	Phase							
Intensity level	Phase 1	Phase 2	Phase 3	Phase 4	Phase 5	Phase 6	Phase 7	Phase 8
ITPV ⩽ 4	14 (19.2%)	15 (18.1%)	22 (23.6%)	20 (28.6%)	24 (32.0%)	26 (50.0%)	21 (44.7%)	18 (30.5%)
4 < ITPV ⩽ 6	24 (32.9%)	27 (32.5%)	19 (20.4%)	24 (34.3%)	27 (36.0%)	13 (25.0%)	14 (29.7%)	18 (30.5%)
6 < ITPV ⩽ 8	19 (26.0%)	19 (22.9%)	34 (36.6%)	15 (21.4%)	16 (21.3%)	8 (15.4%)	10 (21.3%)	15 (25.4%)
ITPV > 8	16 (21.9%)	22 (26.5%)	18 (19.4%)	11 (15.7%)	8 (10.7%)	5 (9.6%)	2 (4.3%)	8 (13.6%)
average ITPV	6.0	6.1	6.2	5.5	5.0	4.5	4.2	5.4

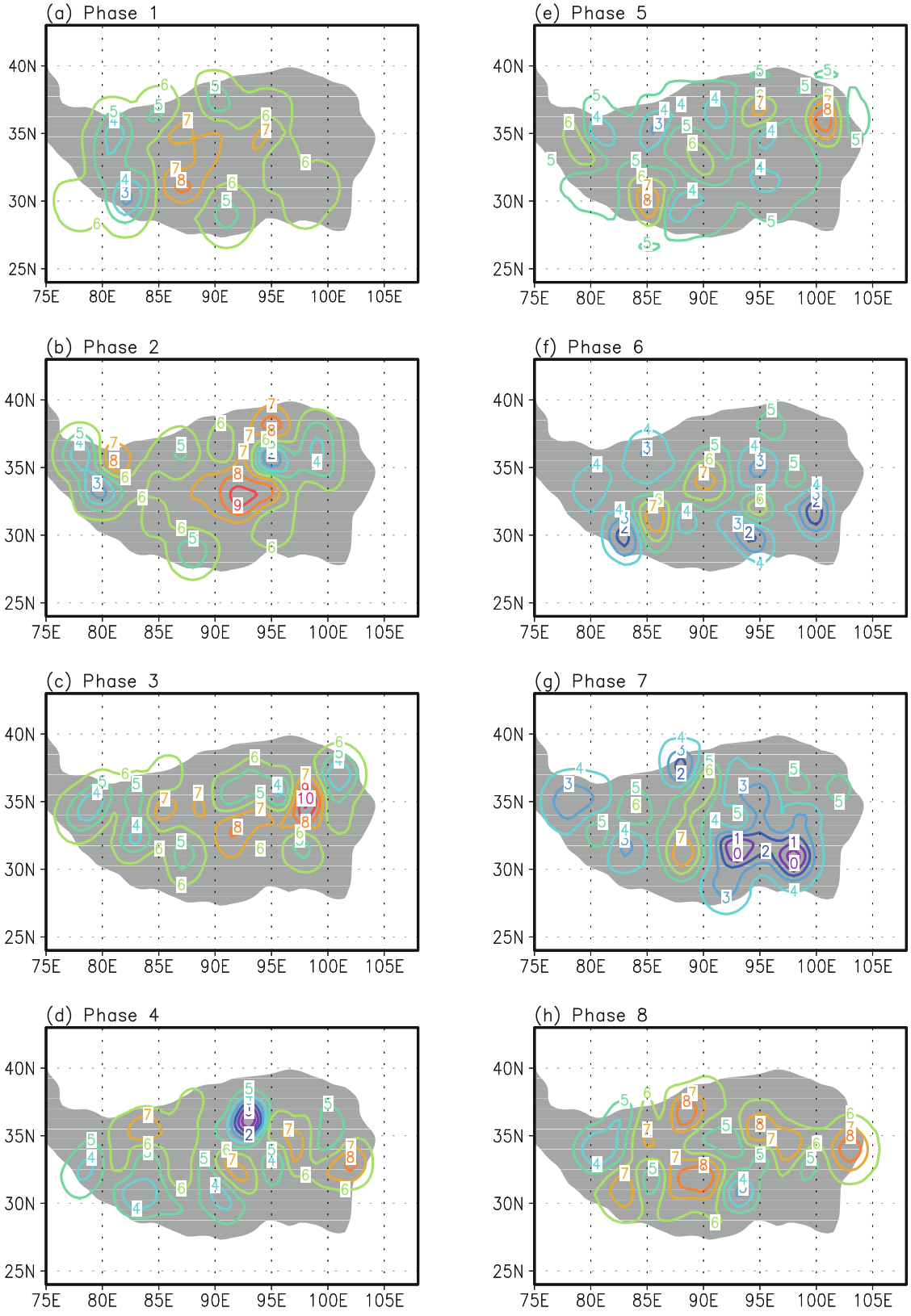

Fig. 3. Spatial distributions of the ITPV in eight phases. The contours represent the intensity of the TPVs (units: 10^{-5} s^{-1}). Altitude higher than 3000 m is shaded to indicate the Tibetan Plateau.

tions of the maximums of the ITPV exhibit an irregular spatial distribution in phases 5–8, and the areas where the ITPV is greater than 6×10^{-5} s^{-1} are much smaller than those in the positive phases. Therefore, the positive QBWO phases provide more favorable conditions for the occurrence of strong TPVs and their eastward expansion.

4. Effect of QBWO on the ITPV

4.1. *Large-scale circulations*

To investigate the large-scale circulations associated with the QBWO, 10–20-day filtered geopotential heights and winds at 500 hPa are composited for the eight QBWO phases (Fig. 4). In the positive phases (phases 2–4), negative geopotential height anomalies over the Tibetan Plateau benefiting the initiation of TPVs are observed. In fact, the negative geopotential height anomalies are strongest in phase 3, in which the average ITPV reaches a maximum (Table 1). Meanwhile, there are two anomalous highs around the Tibetan Plateau. One is found to the west of the Tibetan Plateau and moves eastward, especially in phases 3 and 4. Along with the eastward movement of the anomalous high, the northeasterlies to its east shift eastward and approach the Tibetan Plateau gradually, benefiting the intensification and eastward movement of the anomalous cyclonic circulation over the Tibetan Plateau. Another anomalous high appears to the east of the Tibetan Plateau in phase 3, intensifying the cyclonic wind shear over the central and eastern Tibetan Plateau. Thus, under the coactions of the above three systems, the cyclonic wind shear moves eastward and become strongest in phase 3, corresponding to the highest average ITPV (Table 1) and the locations of the maximums of the ITPV over the eastern Tibetan Plateau in this phase (Fig. 3). In the negative phases (phases 6–8), positive geopotential height anomalies are observed, with a maximum appearing in phase 7. Under the coactions of the negative anomalies to the west and east of the Tibetan Plateau, an anticyclonic wind shear appears over the Tibetan Plateau and gets strongest in phase 7. Therefore, in the positive QBWO phases, the circulations at 500 hPa are conducive to a higher ITPV and the eastward propagation of its maximum centers.

Figure 5 shows the 10–20-day filtered geopotential heights and wind speeds at 200 hPa. In phase 1, an anomalous jet core is found at (43°N, 85°E), and stretches eastward in phases 2–4. Usually, a divergence field can be found on the right-hand side of the entrance of the 200-hPa jet core (Jia and Yang, 2013), which is favorable for the ascending motion over the Tibetan Plateau. In the positive phases, positive geopotential height anomalies are presented over the eastern plateau, and move eastward gradually, contributing to the divergence over the eastern Tibetan Plateau. As shown in Fig. 4, in phases 1–4, the cyclonic wind shears are found over the Tibetan Plateau and become strongest in phase 3, in conjunction with the 200-hPa divergence, and ascending motion is observed over the Tibetan Plateau with the peak appearing in phase 3 (Fig. 6). In fact, as shown in Fig. 6, the ascending motion associated with the 500-hPa convergence and 200-hPa divergence strengthens in phases 1–4, and stretches from the western to the eastern Tibetan Plateau, in accordance with the eastward expansion of the centers of the maximum ITPV (Fig. 3), indicating that the ascending motion is conducive to a higher ITPV. Correspondingly, the highest average ITPV in phase 3 is accompanied by the strongest ascending motion. In phases 5–6, the anomalous jet core and the positive geopotential heights are much farther from the plateau than those in the positive phases. Accordingly, their influence on the ITPV is limited. In phases 7–8, the anomalous jet stream disappears, and there are negative geopotential height anomalies over the eastern Tibetan Plateau, which are not conducive to divergence at 200 hPa. In phases 5–8, anticyclonic wind shears are observed at 500 hPa. Thus, anomalous descending motion controls the Tibetan Plateau in these phases. Overall, the circulations at 500 hPa and 200 hPa, as well as the associated ascending motion, are more conducive to the occurrence of strong TPVs in the positive phases than in the negative phases, which is responsible for a higher ITPV and eastward propagation of the maximum centers of the ITPV in the former.

4.2. *Atmospheric thermodynamic features*

The QBWO of the water vapor condition over the Tibetan Plateau is exhibited in Fig. 7. In the positive phases, the convergence centers of the water vapor propagate eastward in phases 2–4. Notably, the convergence areas of water vapor are in accordance with the locations of the cyclonic wind shear, and the vectors of water vapor flux correspond well to the wind fields at 500 hPa (Fig. 4), implying the importance of the 500-hPa wind fields for water vapor transportation. The warm and wet water vapor from the Arabian Sea is transported to the Tibetan Plateau, which is favorable for unstable stratification and precipitation. In the negative phases, the water vapor divergence centers over the Tibetan Plateau move eastward, contributing to stable stratification over the plateau. Thus, the water vapor condition over the Tibetan Plateau in the positive phases is beneficial to increasing the atmospheric instability and provides favorable conditions for precipitation, which is helpful for intensifying the low-pressure systems.

The atmospheric stratification stability over the Tibetan Plateau in the eight QBWO phases is investigated by analyzing the vertical distributions of the 10–20-day filtered potential pseudo-equivalent temperature (θ_{se}) averaged between 32°N and 36°N (Fig. 8). Positive θ_{se} anomalies to the west of the Tibetan Plateau move onto the plateau in phase 1, with the centers located at approximately 500 hPa and near 83°E, indicating unstable stratification over the western plateau. The positive θ_{se} anomaly centers located over the Tibetan Plateau stretch eastward in phases 1–3 and reach a maximum in phase 3, implying that the unstable conditions move eastward and the strongest unstable stratification appears in phase 3. In phase 4, most parts of the positive θ_{se} anomalies have deviated from the plateau. In phase 5, a negative anomalous θ_{se} center is observed over the western Tibetan Plateau below 400 hPa, and then it strengthens and moves eastward in phases 6–8. The intensity of the negative anomalous θ_{se} center peaks in phase 7, indicating the most stable stratification is reached in this phase. Usually, positive θ_{se} anomalies mean warm and humid air over the Tibetan Plateau, providing favorable conditions for the generation of strong TPVs. Thus, in the positive phases, the average ITPV is higher, and the locations of positive θ_{se} anomalies centers coincide with the

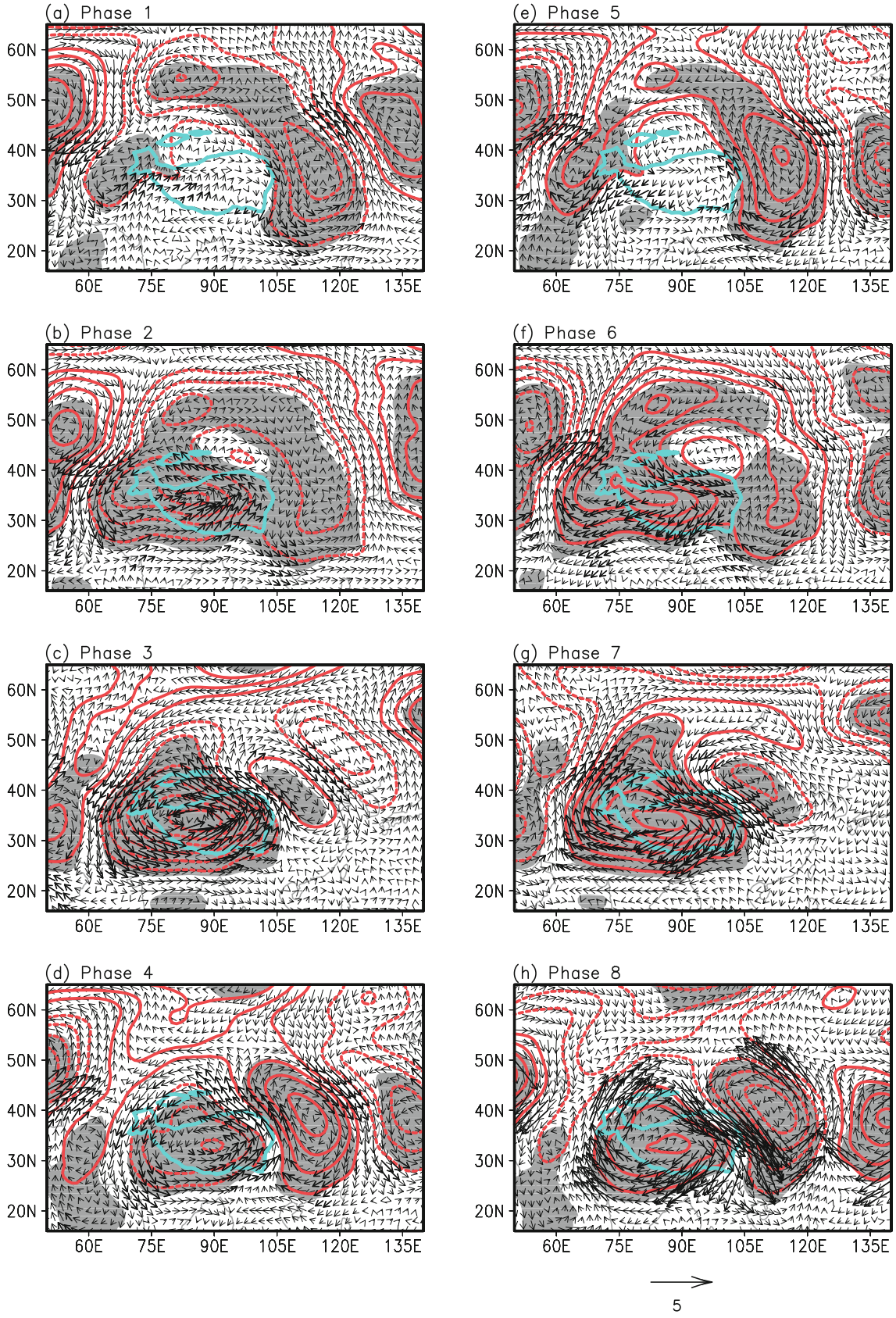

Fig. 4. Composites of 10–20-day filtered 500-hPa geopotential heights (red contours; units: gpm; interval of contours: 3 gpm) and winds (vectors; units: m s^{-1}) for eight phases. The geopotential heights and winds passing the 95% confidence level are shaded and colored black, respectively. The blue solid line with topography of 3000 m indicates the scope of the Tibetan Plateau.

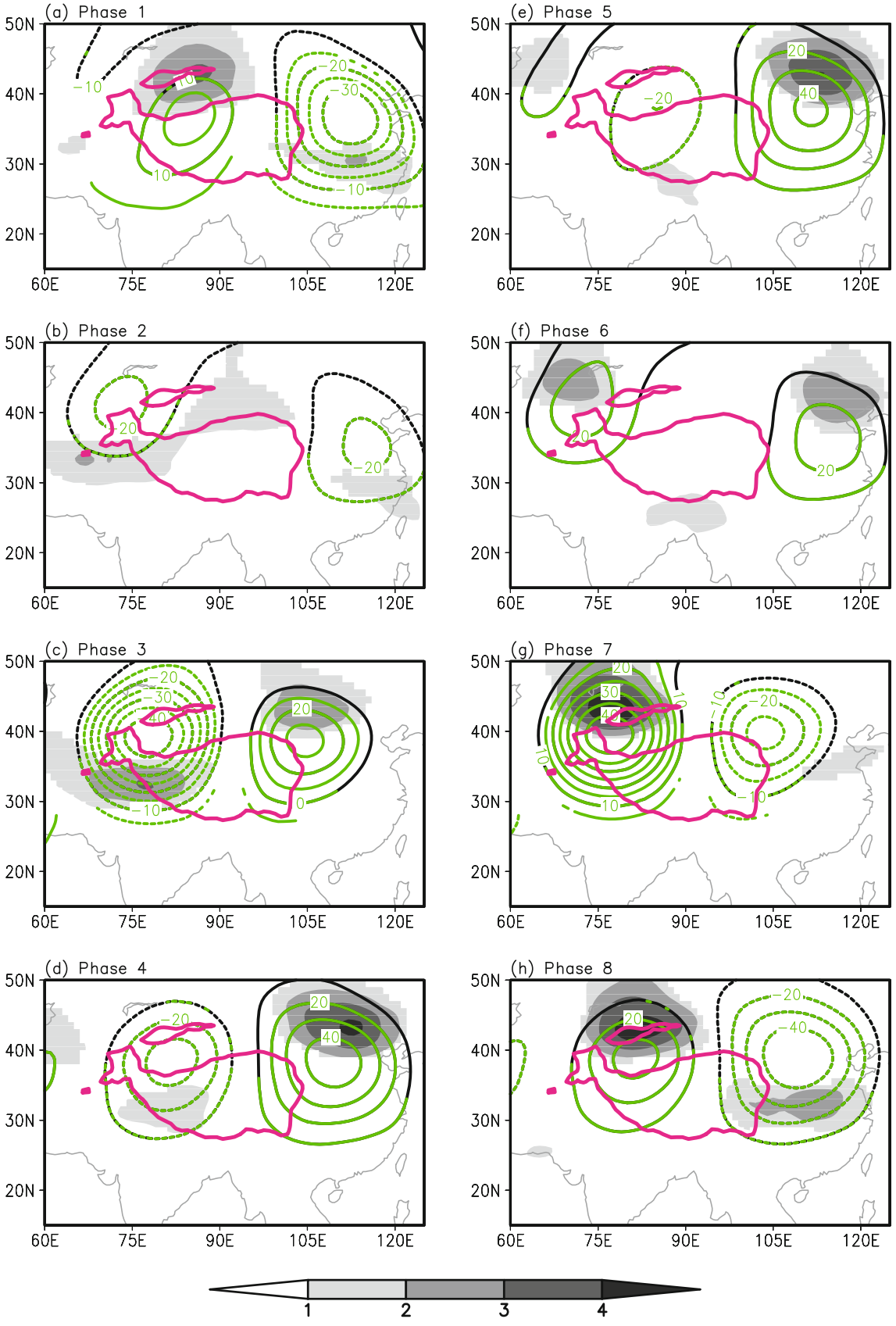

Fig. 5. As in Fig. 4 but for 200-hPa wind speeds (shaded; units: m s^{-1}) and geopotential heights (contours; units: gpm). The geopotential heights passing the 95% confidence level are colored green, and wind speeds below the 95% confidence level are omitted. The red solid line with topography of 3000 m indicates the scope of the Tibetan Plateau.

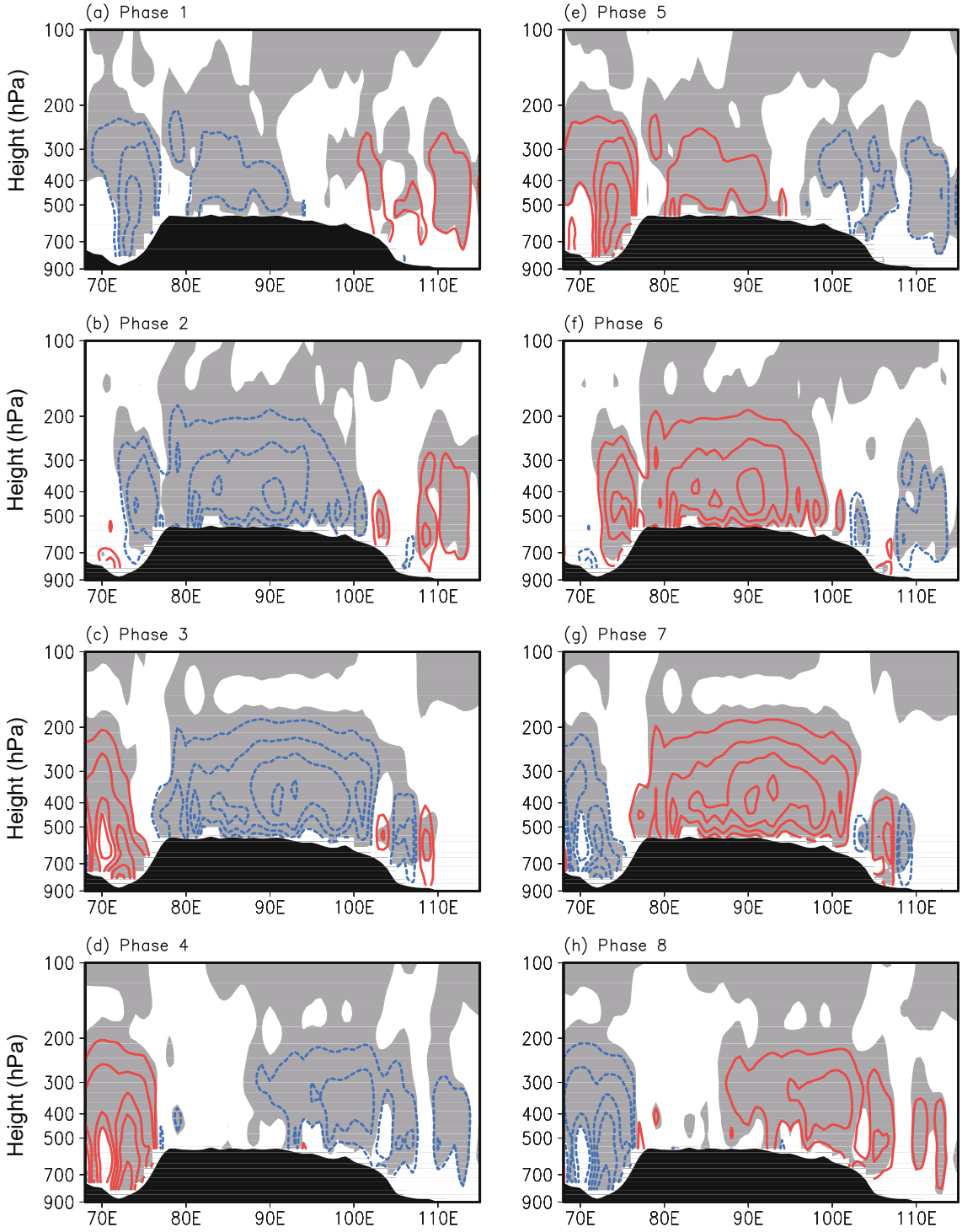

Fig. 6. Height-longitude cross-sections of the vertical velocity (contours; units: pa s^{-1}) averaged between 32°N and 36°N for eight phases. The positive values are represented by red contours, and the negative values are colored blue. The intervals of both the red and blue contours are 0.01 pa s^{-1}. The vertical velocity passing the 95% confidence level is shaded gray. Black shading denotes the topography.

eastward propagation of the maximums of the ITPV. In contrast, negative θ_{se} anomalies indicate cold and dry air, leading to a lower ITPV.

According to the analyses above, in the positive phases, the cyclonic wind shears at 500 hPa strengthen and move eastward, while the divergence associated with the anomalous high and the jet stream are located at 200 hPa, resulting in an eastward moving ascending motion with the intensity reaching a peak in phase 3. Meanwhile, there are clear eastward shifting water vapor convergence centers and unstable stratification over the Tibetan Plateau. All of these conditions are conducive to precipitation, which is closely related to the

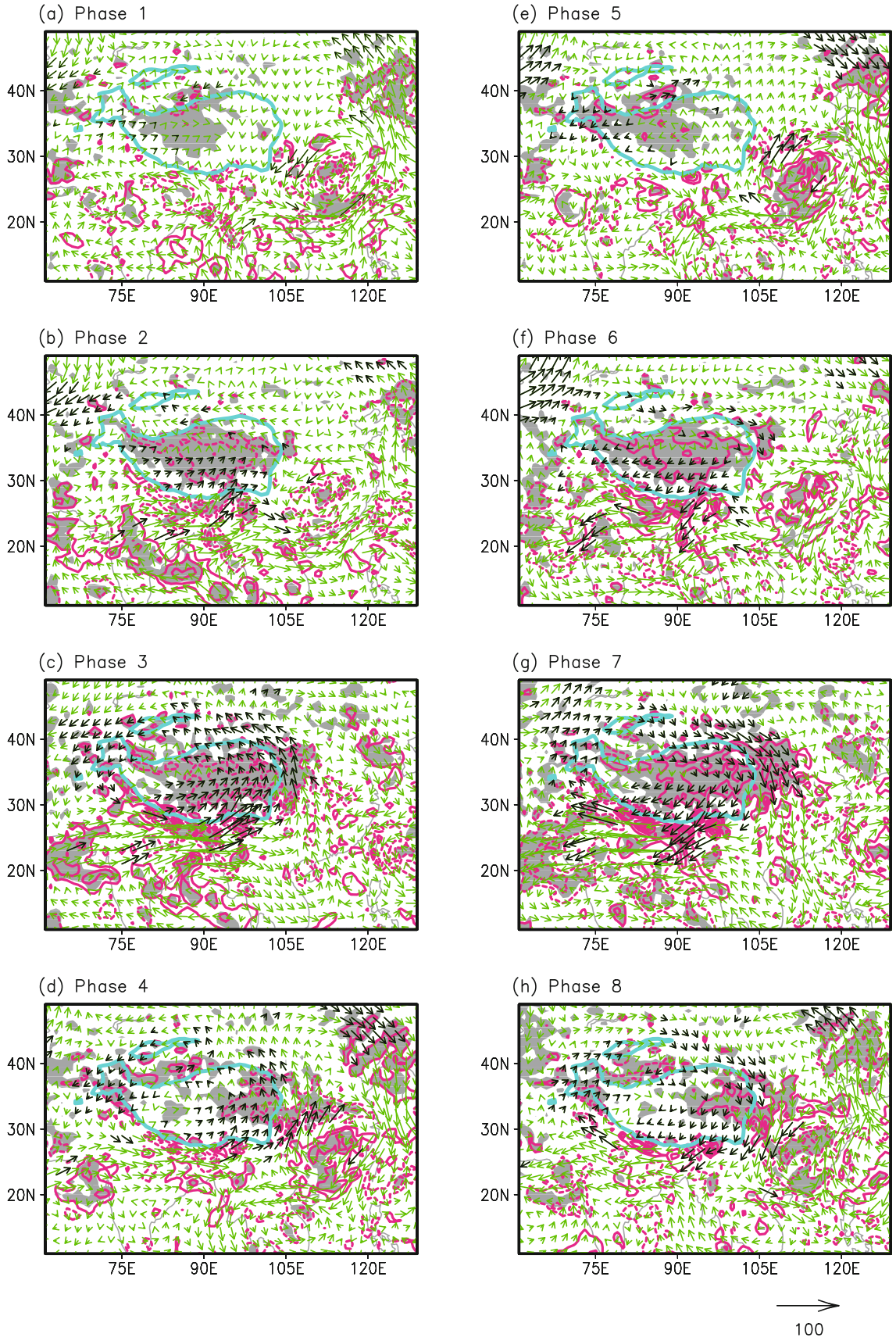

Fig. 7. As in Fig. 4 but for vertically integrated water vapor flux (vectors; units: kg m^{-1} s^{-1}) and water vapor flux divergence (contours; units: 10^{-5} kg m^{-2} s^{-1}). Water vapor flux and water vapor flux divergence passing the 95% confidence level is colored black and shaded, respectively.

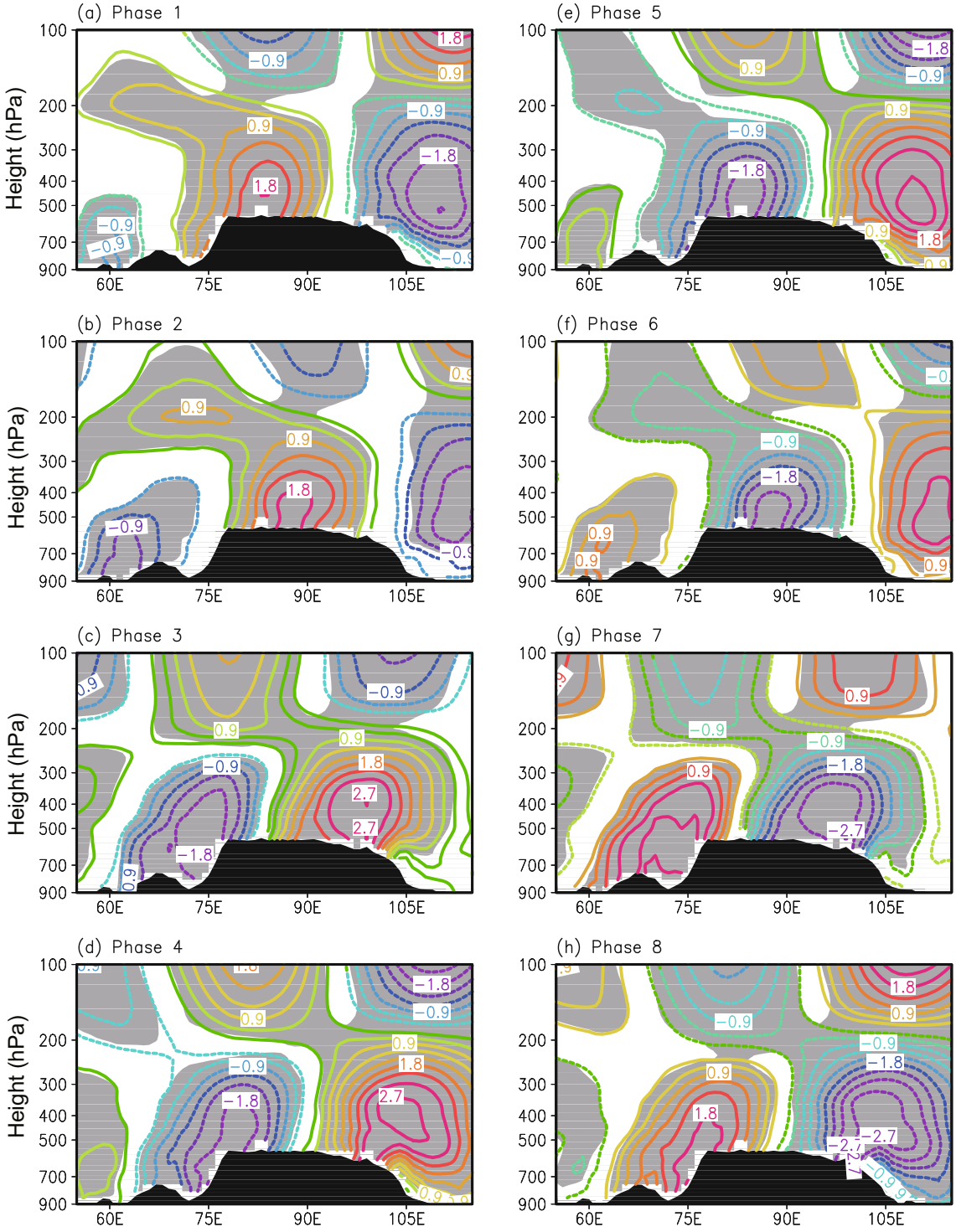

Fig. 8. As in Fig. 6 but for potential pseudo-equivalent temperature (θ_{se}) (units: K). θ_{se} passing the 95% confidence level is shaded gray.

release of condensational latent heat. The heating fields are discussed below.

Figure 9 presents the features of 10–20-day filtered Q_1 and Q_2 averaged between 32°N and 36°N. In phase 1, positive (negative) Q_1 and Q_2 anomalies are found over the western (eastern) Tibetan Plateau. Then, the positive ones intensify and move eastward to the central and eastern plateau. In phases 2–4, the vertical distributions of the positive anomalous Q_1 and Q_2 are similar, and their heating centers are both located at approximately 400 hPa, implying that Q_1 is mainly sourced from the condensational latent heat. In phase 3, the intensities of Q_1 and Q_2 reach their maximums, coinciding with the highest average ITPV (Table 1), while the zonal heating range of Q_2 corresponds to high ITPV centers be-

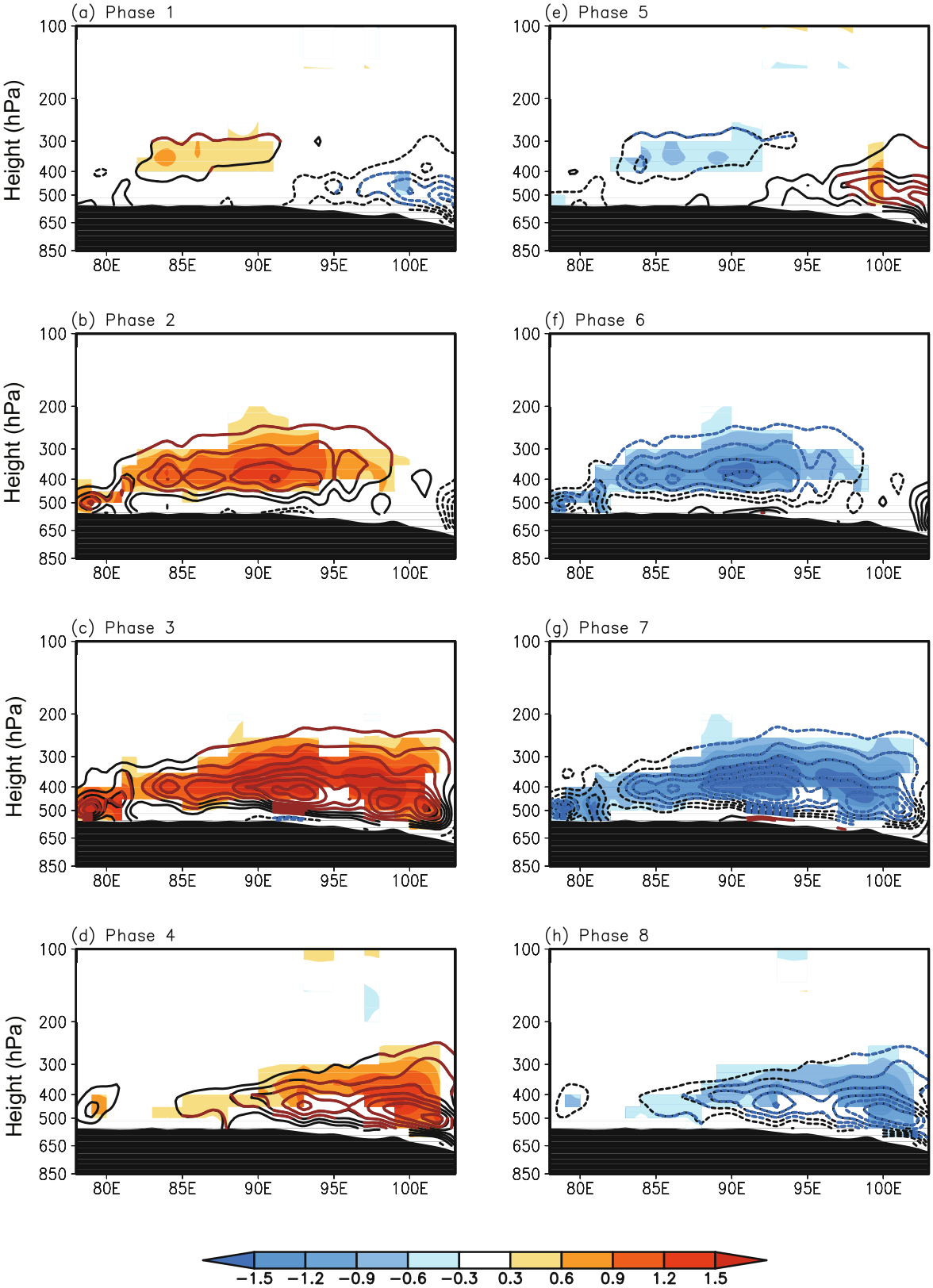

Fig. 9. As in Fig. 6 but for the atmospheric apparent heat source (Q_1) (colored shading; units: K d^{-1}) and apparent moisture sink (Q_2) (black contours; units: K d^{-1}; interval of the contours: 0.3 K d^{-1}). Q_1 below the 95% confidence level is omitted, while Q_2 passing the 95% confidence level is colored red for positive values and blue for negative values.

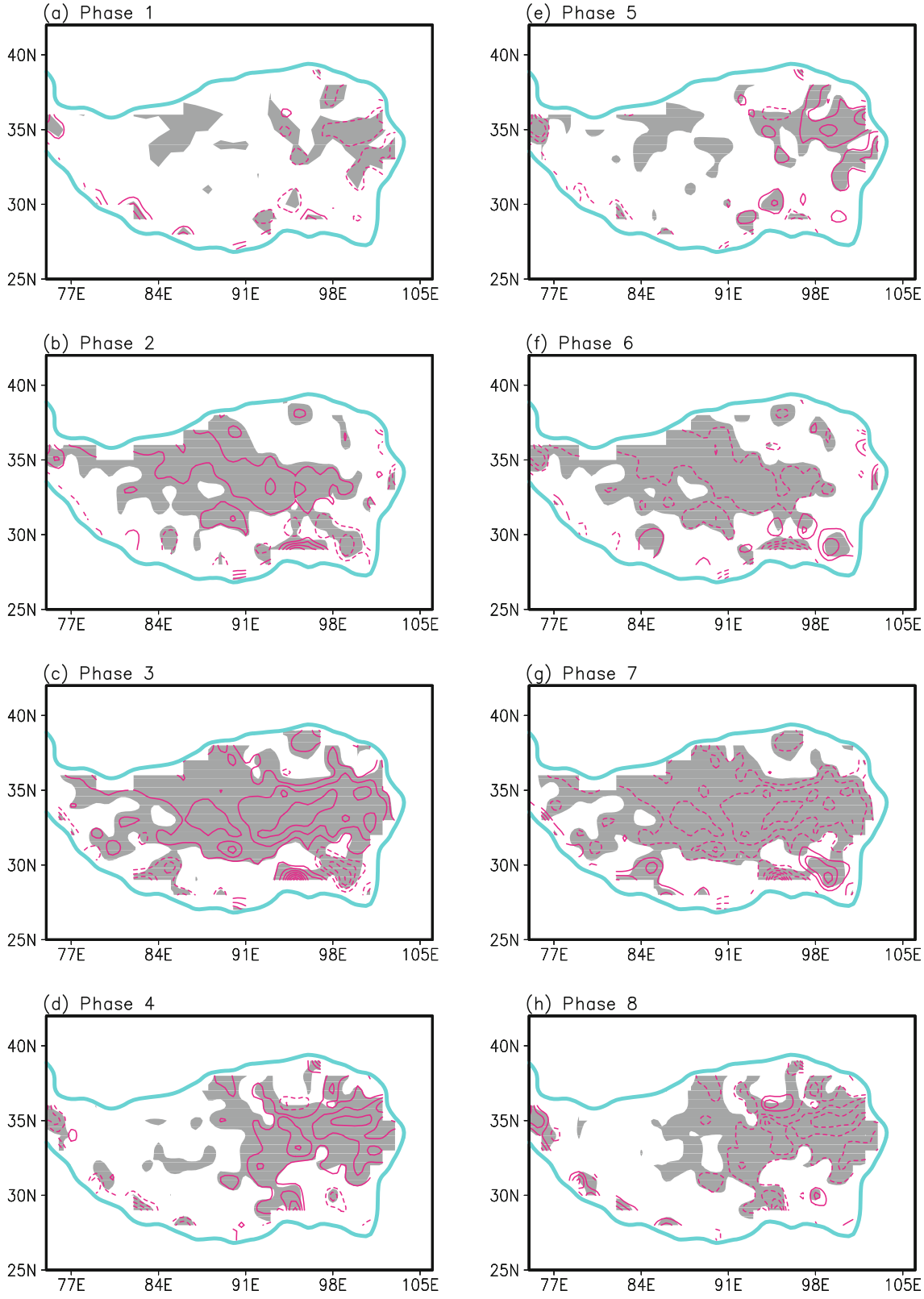

Fig. 10. As in Fig. 4 but for the vertically integrated atmospheric apparent moisture sink ($\langle Q_2 \rangle$) (units: K d^{-1}; interval of contours: 20 K d^{-1}). $\langle Q_2 \rangle$ passing the 95% confidence level is shaded.

tween 90°E and 100°E in Fig. 3. Latent heating above 500 hPa can strengthen TPVs by depressing the 500-hPa isobaric surface, contributing to a higher ITPV (Li et al., 2011). In the negative phases, negative Q_1 and Q_2 anomalies cover most of the Tibetan Plateau, which hinder the formation processes of the TPVs. The role of the condensational latent heat can

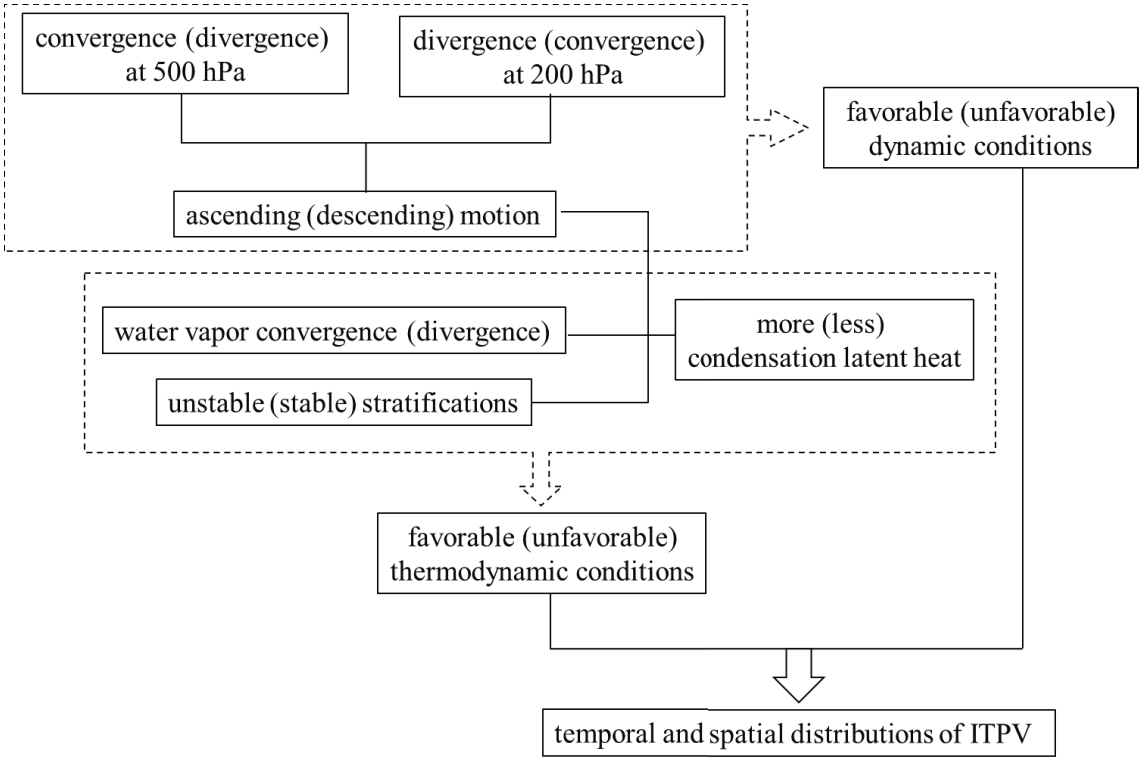

Fig. 11. Conceptual diagram illustrating the mechanism by which the QBWO modulates the ITPV. The situation given in parentheses is for negative phases.

be further verified in Fig. 10, in which the anomalous vertically integrated Q_2 ($\langle Q_2 \rangle$) in the eight phases are shown. In the positive phases, centers of the positive $\langle Q_2 \rangle$ anomalies stretch eastward over the Tibetan Plateau, whose ranges are in accordance with the distributions of high ITPV shown in Fig. 3. Therefore, the condensational latent heat has a significant impact on the ITPV and its eastward propagation over the Tibetan Plateau.

To clearly show the mechanism by which the QBWO modulates the ITPV, a conceptual diagram is presented in Fig. 11. In the positive phases, the anomalous convergence at 500 hPa, the divergence at 200 hPa, and the associated ascending motion, are favorable dynamic factors for generating a higher ITPV. In addition, anomalous water vapor convergence and unstable atmospheric stratification in the positive phases, in conjunction with the favorable dynamic conditions, result in precipitation and the related condensational latent heat, which is conducive to the initiation of TPVs. Meanwhile, stronger TPVs lead to heavier precipitation and more intensive condensational latent heating in turn, exhibiting a feedback relationship between the TPVs and the precipitation (Wang, 1987; Li et al., 2014b). In the negative phases, the situation is opposite. Here, it should be clarified that TPVs are important factors in triggering precipitation, but are not the only reason for precipitation. Thus, in the present work, it is considered that the condensational latent heat, which exerts a vital influence on TPVs, is caused by the coactions of the ascending motion, the water vapor conditions, and the unstable atmospheric stratification over the Tibetan Plateau.

5. Conclusions and discussion

In this work, the modulation of the ITPV by the QBWO is investigated based on NCEP FNL data, and the dynamic and thermodynamic conditions related to the QBWO are further analyzed to reveal the physical processes underlying the modulation of the spatial and temporal distributions of the ITPV by the QBWO. The main results are as follows:

The spatial and temporal distributions of the ITPV show distinct features of 10–20-day QBWO. The number of strong TPVs (intensity greater than 6×10^{-5} m s^{-1}) in the positive QBWO phases is much larger than that in the negative phases, and the largest and smallest numbers appear in phases 3 and 7, respectively. In addition, the average ITPV peaks in phase 3, while the minimum appears in phase 7. The spatial distributions of the ITPV in the eight QBWO phases show that the maximum centers of the ITPV shift eastward in the positive phases, and the largest ITPV is located over the eastern Tibetan Plateau in phase 3. In the negative phases, the occurrence locations of strong TPVs are irregular.

The ITPV is modulated by the dynamic and thermodynamic fields of the 10–20-day QBWO. In the positive phases, eastward shifting anomalous cyclonic wind shears over the Tibetan Plateau are found at 500 hPa. In addition, there is divergence associated with the eastward stretching anomalous jet stream and positive geopotential height at 200 hPa. The divergence at 200 hPa and convergence at 500 hPa are beneficial to the ascending motion. In thermodynamic fields, the water vapor converges to the Tibetan Plateau in the posi-

tive phases, and the convergence centers propagate eastward. Additionally, eastward shifting atmospheric unstable stratification is found over the Tibetan Plateau. The ascending motion, the water vapor convergence, and the unstable conditions propagate eastward and become strongest in phase 3, which is conducive to precipitation and related latent heat release. The heating centers around 400 hPa benefit a higher ITPV by depressing the 500-hPa isobaric surface. Thus, in the positive phases, the range of the condensational latent heating is in accordance with the distribution of the centers of the ITPV, indicating an important effect of the latent heat on the eastward propagation of the initial locations of strong TPVs. The strongest heating in phase 3 corresponds to the highest average ITPV in that phase. In contrast, in the negative phases, there is anomalous descending motion, stable stratification, and water vapor divergence; thus, anomalous cooling fields are found in these phases, hindering the initiation processes of TPVs. Therefore, the average ITPV in the positive phases is much higher than that in the negative phases.

In this study, we mainly focused on the effect of the QBWO over the Tibetan Plateau; the origin of the QBWO is not investigated. Thus, the origin of the QBWO over the Tibetan Plateau and how systems from lower and higher latitudes influence it requires further research.

Acknowledgements. The authors are grateful to the anonymous reviewers for their advice regarding this study. This work is supported by the National Key Research and Development Program (Grant Nos. 2016YFA0601504 and 2016YFA0600602), the National Natural Science Foundation of China (Grant No. 41775059), the China National 973 Project (Grant No. 2015CB453203), the Basic Scientific Research and Operation Foundation of CAMS (Grant Nos. 2016Y001 and 2018Z006), and the Science and Technology Development Fund of CAMS (Grant No. 2018KJ029).

REFERENCES

Chen, B. M., Z. A. Qian, and L. S. Zhang, 1996: Numerical simulation of the formation and development of vortices over the Qinghai-Xizang Plateau in summer. *Scientia Atmospherica Sinica*, **20**, 491–502, https://doi.org/10.3878/j.issn.1006-9895.1996.04.14. (in Chinese with English abstract)

Dell'Osso, L., and S. J. Chen, 1986: Numerical experiments on the genesis of vortices Over the Qinghai-Tibet Plateau. *Tellus A*, **38**, 236–250, https://doi.org/10.1111/j.1600-0870.1986.tb00468.x.

Duchon C. E., 1979: Lanczos filtering in one and two dimensions. *J. Appl. Meteor.*, **18**, 1016–1022, https://doi.org/10.1175/1520-0450(1979)018<1016:LFIOAT>2.0.CO;2.

Jia, X. L., and S. Yang, 2013: Impact of the quasi-biweekly oscillation over the western North Pacific on East Asian subtropical monsoon during early summer. *J. Geophys. Res. Atmos.*, **118**, 4421–4434, https://doi.org/10.1002/jgrd.50422.

Lhasa Group for Tibetan Plateau Meteorology Research, 1981: *Research of 500 hPa Shear Lines over the Tibetan Plateau in Summer.* Science Press, 122 pp. (in Chinese)

Li, G. P., 2002: *Dynamic Meteorology of the Tibetan Plateau*. China Meteorological Press, 271 pp. (in Chinese)

Li, G. P., B. J. Zhao, and J. Q. Yang, 2002: A dynamical study of the role of surface sensible heating in the structure and intensification of the Tibetan Plateau vortices. *Chinese Journal of Atmospheric Sciences*, **26**, 519–525, https://doi.org/10.3878/j.issn.1006-9895.2002.04.09. (in Chinese with English abstract)

Li, L., R. H. Zhang, and M. Wen, 2011: Diagnostic analysis of the evolution mechanism for a vortex over the Tibetan Plateau in June 2008. *Adv. Atmos. Sci.*, **28**(4), 797–808, https://doi.org/10.1007/s00376-010-0027-y.

Li, L., R. H. Zhang, and M. Wen, 2014a. Diurnal variation in the occurrence frequency of the Tibetan Plateau vortices. *Meteor. Atmos. Phys.*, **125**, 135–144, https://doi.org/10.1007/s00703-014-0325-5.

Li, L., R. H. Zhang, M. Wen, and L. K. Liu, 2014b: Effect of the atmospheric heat source on the development and eastward movement of the Tibetan Plateau vortices. *Tellus A*, **66**, 24451, https://doi.org/10.3402/tellusa.v66.24451.

Li, L., R. H. Zhang, M. Wen, and J. M. Lü, 2018a: Effect of the atmospheric quasi-biweekly oscillation on the vortices moving off the Tibetan Plateau. *Clim. Dyn.*, **50**, 1193–1207, https://doi.org/10.1007/s00382-017-3672-3.

Li, L., R. H. Zhang, and M. Wen, 2017: Genesis of southwest vortices and its relation to Tibetan Plateau vortices. *Quart. J. Roy. Meteor. Soc.*, **143**, 2556–2566, https://doi.org/10.1002/qj.3106.

Li, L., R. H. Zhang, and M. Wen, 2018b: Modulation of the atmospheric quasi-biweekly oscillation on the diurnal variation of the occurrence frequency of the Tibetan Plateau vortices. *Climate Dyn.*, **50**, 4507–4518, https://doi.org/10.1007/s00382-017-3887-3.

Luo, S. W., 1992: *Study on Some Kinds of Weather Systems Over and Around the Qinghai-Xizang Plateau*. China Meteorological Press, 7–55. (in Chinese)

Luo, S. W., M. L. He, and X. D. Liu, 1994: Study on the vortex of the Qinghai-Xizang (Tibet) Plateau in summer. *Science in China Series B*, **37**, 601–612.

Luo, S. W., and Y. Yang, 1992: A case study on numerical simulation of summer vortex over Qinghai-Xizang (Tibetan) Plateau. *Plateau Meteorology*, **11**, 39–48. (in Chinese with English abstract)

Luo, S. W., Y. Yang, and S. H. Lü, 1991: Diagnostic analyses of a summer vortex over Qinghai-Xizang Plateau for 29-30 June 1979. *Plateau Meteorology*, **10**, 1–12. (in Chinese with English abstract)

Qiao, Q. M., and Y. G. Zhang, 1994: *Synoptic Meteorology of the Tibetan Plateau and Its Effect on the Near Areas.* China Meteorological Press, 120–155. (in Chinese)

Rasmusson, E. M., 1968: Atmospheric water vapor transport and the water balance of north America II. Large-scale water balance investigations. *Mon. Wea. Rev*., **96**, 720–734, https://doi.org/10.1175/1520-0493(1968)096<0720:AWVTAT>2.0.CO;2.

Shen, R. J., E. R. Reiter, and J. F. Bresch, 1986: Some aspects of the effects of sensible heating on the development of summer weather systems over the Tibetan Plateau. *J. Atmos. Sci*., **43**, 2241–2260, https://doi.org/10.1175/1520-0469(1986)043<2241:SAOTEO>2.0.CO;2.

Sun, G. W., and B. D. Chen, 1994: Characteristics of the lows flocking with Tibet atmospheric low-frequency oscillation over the Qinghai-Xizang (Tibet) Plateau. *Scientia Atmospher-*

ica Sinica, **18**, 113–121, https://doi.org/10.3878/j.issn.1006-9895.1994.01.14. (in Chinese with English abstract)

Tu, N. N., and G. B. He, 2010: Case analysis on two low vortexes induced by Tibetan Plateau shear line. *Plateau Meteorology*, **29**, 90–98. (in Chinese with English abstract)

Wang, B., 1987: The development mechanism for Tibetan Plateau warm vortices. *J. Atmos. Sci.*, **44**, 2978–2994, https://doi.org/10.1175/1520-0469(1987)044<2978:TDMFTP>2.0.CO;2.

Wang, X., Y. Q. Li, S. H. Yu, and X. W. Jiang, 2009: Statistical study on the plateau low vortex activities. *Plateau Meteorology*, **28**, 64–71. (in Chinese with English abstract)

Yanai, M., E. Steven, and J. H. Chu, 1973: Determination of bulk properties of tropical cloud clusters from large-scale heat and moisture budgets. *J. Atmos. Sci.*, **30**, 611–627, https://doi.org/10.1175/1520-0469(1973)030<0611:DOBPOT>2.0.CO;2.

Ye, D. Z., and Y. X. Gao, 1979: *The Tibetan Plateau Meteorology*. Science Press, 278 pp. (in Chinese)

Yu, S. H., and G. B. He, 2001: Numerical experiment of influence of water vapor in the middle and upper troposphere on the formation of vortex over the Tibetan Plateau. *Journal of Nanjing Institute of Meteorology*, **24**, 553–559, https://doi.org/10.3969/j.issn.1674-7097.2001.04.014. (in Chinese with English abstract)

Zhang, P. F., G. P. Li, X. H. Fu, Y. M. Liu, and L. F. Li, 2014: Clustering of Tibetan Plateau vortices by 10-30-day intraseasonal oscillation. *Mon. Wea. Rev.*, **142**, 290–300, https://doi.org/10.1175/MWR-D-13-00137.1.

Zheng, Y. J., G. X. Wu, and Y. M. Liu, 2013: Dynamical and thermal problems in vortex development and movement. Part I: A PV–Q view. *Acta Meteorologica Sinica*, **27**, 1–14, https://doi.org/10.1007/s13351-013-0101-3.